Research Article | Vol. 29, No. 21 / 11 Oct 2021 / Optics Express 32755
Optics EXPRESS

# Highly efficient vertical coupling to a topological waveguide with defect structure

HIBIKI KAGAMI,[1,4] TOMOHIRO AMEMIYA,[1,2,5] SHO OKADA,[1] NOBUHIKO NISHIYAMA,[1,2] AND XIAO HU[3,6]

[1]*Department of Electrical and Electronic Engineering, Tokyo Institute of Technology, Tokyo 152-8552, Japan*
[2]*Institute of Innovative Research (IIR), Tokyo Institute of Technology, Tokyo 152-8552, Japan*
[3]*International Center for Materials Nanoarchitectonics (WPI-MANA), National Institute for Materials Science, Tsukuba 305-0044, Japan*
[4]*kagami.h.aa@m.titech.ac.jp*
[5]*amemiya.t.ab@m.titech.ac.jp*
[6]*hu.xiao@nims.go.jp*

**Abstract:** In this study, we propose a defect structure that enhances the vertical coupling efficiency of circularly polarized light incident on topological waveguides consisting of triangle nanoholes with $C_{6v}$ symmetry arranged in honeycomb lattice. The defect structure was formed by removing triangle nanoholes from a certain hexagonal unit cell around the topological waveguide. As a result of comparing the coupling efficiency with and without the defect structure through three-dimensional finite-difference time-domain analysis, significant improvement in the vertical coupling efficiency was observed over the entire telecom C band (4460%@1530 nm). In addition, it was also found that the wavelength showing maximum coupling efficiency can be controlled over the entire C band by changing the arrangement of the dielectric around the defect structure.



## 1. Introduction

Tracing the topology of electronic systems represented by topological insulators [1–4] to photon systems is called "topological photonics" which has been progressing rapidly in recent years [5–22]. Topological photonic systems can be realized by constructing a unit cell of periodic photonic nanostructure with multiple dielectrics, and it is possible to produce photonic bands with topological features by controlling the interactions within and between the unit cells [9,23]. Photonic crystals [24–28] and metamaterials [29–36] have been widely studied as similar periodic nanostructures, but the former primarily uses interactions between the cells, whereas the latter uses interactions within the cells. In contrast, topological photonics systems have a greater degree of freedom for interactions, making it possible to design photonic bands more flexibly [37–40].

The most prominent phenomenon in topological photonics systems is the existence of edge states that transport electromagnetic waves in a unidirectional way. In the honeycomb-type semiconductor photonic crystals (PhCs) the topological edge states are governed by the pseudospin-momentum locking mimic the quantum spin Hall effect in electron systems, where the optical pseudospin degree of freedom is defined based on the phase winding of eigen modes in the photonic structures [9,41–43]. It is intriguing to ask whether these topological waveguides can be exploited as on-chip and passive multiplex/demultiplex devices for lights carrying on phase winding such as spin (i.e. polarization of light) and vortex (i.e. orbital angular momentum) [44,45], which are considered as indispensable elements for large-capacity optical transmission in future [46–49].

There is an obvious hurdle to be overcome for achieving this goal. The pseudospin in the topological PhC is defined in two dimensions based on TM or TE modes [9,23], whereas the light polarization and optical vortex are generally considered in three dimensions, which do

#432964 https://doi.org/10.1364/OE.432964
Journal © 2021 Received 4 Jun 2021; revised 27 Aug 2021; accepted 9 Sep 2021; published 27 Sep 2021

Optics EXPRESS

not have high affinity with each other. Therefore, it is necessary to clarify how to direct lights carrying on spin and/or vortex from free space vertically to the topological waveguide in an efficient way. For horizontal coupling it has been reported that a topological converter [50] and a polarity-matching structure [51] can allow highly efficient coupling from a normal optical waveguide to a topological waveguide.

In this study, we report that highly efficient vertical coupling can be achieved by introducing a defect structure around the topological waveguide. We first discuss whether the vertical coupling efficiency depends on a defect structure (Section 2). Next, we evaluate how the coupling efficiency changes depending on the location of the defect structure (Section 3). Finally, we show that the wavelength showing the maximum coupling efficiency can be controlled by tuning the arrangement of the dielectric around the defect structure (Section 4). The details of these are described below.

## 2. Improvement of vertical coupling efficiency by introducing a defect structure

The proposed device structure is shown in Fig. 1(a). In this study we constructed a topological waveguide by interfacing a topological PhC and a trivial PhC, both formed by triangle nanoholes arranged in honeycomb-type structures respecting $C_{6v}$ symmetry [9]. For the sake of simplicity, an air bridge structure is assumed in which a dielectric layer with a high refractive index is sandwiched between air clads.

In the above structure, the vertical coupling efficiency can be improved by removing triangular nanoholes from a hexagonal unit cell, thus forming a defect for the PhC, around the topological waveguide, as shown in Fig. 1(b) (hereinafter referred to as 'defect structure'). In this defect structure, as the air holes are filled with dielectrics having a higher refractive index than air, it becomes a cavity that firmly traps the vertical incident light. At the same time, the trapped light can couple with the topological waveguide with high efficiency depending on defect position relative to the interface between two PhCs.

In this study, the dielectric layer was made of Si with a thickness of 220 nm. The two PhCs distinct in topology were realized by changing the distance $R$ from the center of the hexagonal unit cell to the center of the nanoholes, and the length $L$ of one side of the nanohole. In particular, we used the two structures $(R, L) = (250\ \text{nm}, 250\ \text{nm})$ and $(290\ \text{nm}, 250\ \text{nm})$, for the trivial PhC and topological PhC respectively, with a common lattice constant $a_0 = 825$ nm (See Fig. 1(c)), which share the same frequency band gap at 1500–1600 nm based on the band diagram calculations using plane wave expansion (PWE).

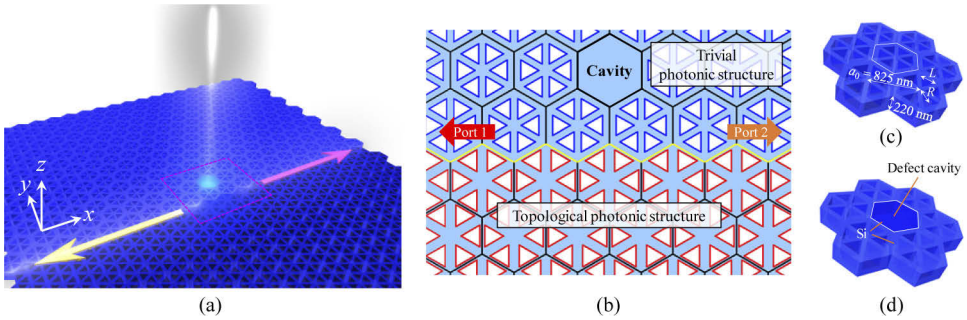


**Fig. 1.** (a) Schematic image of vertical coupling from free space to a topological waveguide. (b) Defect structure for improving vertical coupling efficiency where triangular nanoholes are removed from a hexagonal unit cell close to the topological waveguide. (c) and (d) Schematic image of defect structure where geometrical parameters are shown.

Optics EXPRESS

In simulations (using R-soft) for the transmission along the topological interface channel under an incident light, we used the three-dimensional finite-difference time-domain method (FDTD), and light was made to fall on the center of the defect structure with a beam waist diameter of $1.25a_0$ by placing a focal lens 1.5 μm above the device. Here, the incident light was composed by a gaussian beam. Figure 2(a) shows the calculated output intensity at port 1 when right circularly polarized light was incident on the device. As a result, a significant improvement in the vertical coupling efficiency upon introducing a defect cavity (See Fig. 1(d)) was observed for the entire band ranging from 1500 nm to 1600 nm, where the topological edge state occurs, and a maximum increase of 4460% in output intensity was confirmed at a wavelength of 1530 nm.

In order to understand these results, we performed computer simulations on the topological edge state propagating from right to left which is launched by a source located at the interface far away from the defect, whereas the vertical incident beam is absent. Figure 2(b) shows the mode distribution of out-of-plane magnetic field ($H_z$) of a topological edge state at a wavelength of 1530 nm. As can be seen in Fig. 2(c), a zoomed-in picture at the defect structure in Fig. 2(b), and 2(d), the distribution of $H_z$ inside the defect is almost the same as the distribution of the magnetic field $H_z$ of a right circularly polarized beam incident to the topological waveguide shown in Fig. 1(a). This mode matching facilitates an efficient conversion from the right circularly polarized beam propagating in free space to the guided wave passing through the topological waveguide, as displayed in Fig. 2(a).

Figure 3 shows the mode distributions of the propagating light at several typical wavelengths given in Fig. 2(a). At wavelengths within the band where the topological edge state occurs, the vertically incident light coupled more strongly to the waveguide with the defect structure as compared to the case without the defect structure, and unidirectional propagation for the circularly polarized light was confirmed (propagation in the opposite direction along the interface was almost completely blocked). On the other hand, at wavelengths outside the band where the topological edge state occurs, we found that the light spreads over the entire structure, which is natural since the two PhCs are transparent at those frequencies.

Figures 4(a) and 4(b) show the wavelength dependence of the output intensity at the two ports when left and right circularly polarized light is incident, respectively, on the device as

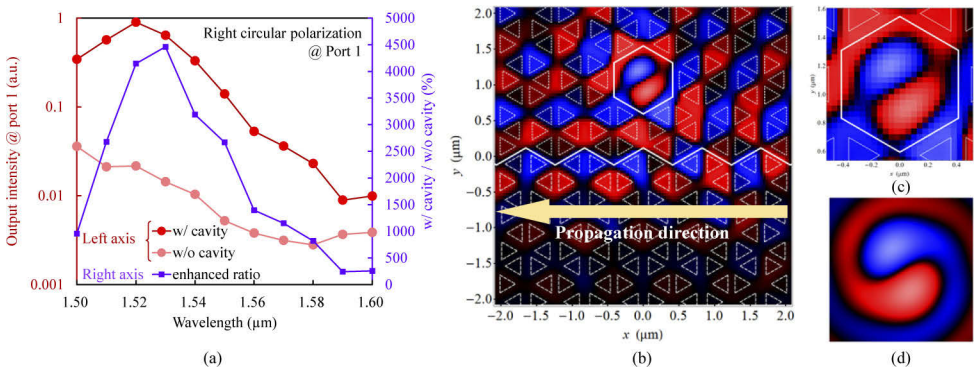


**Fig. 2.** (a) Calculated output intensity at port 1 when right circularly polarized light was incident to the device as shown in Fig. 1(b). (b) Calculated out-of-plane magnetic distribution ($H_z$) of the topological interface state at a wavelength of 1530 nm launched by a source located at the interface and far away the defect structure in the x direction when incident beam is absent. (c) Distribution of $H_z$ inside the defect shown in (b). (d) Distribution of the magnetic field of a right circularly polarized beam in the plane perpendicular to the propagating direction. (See Visualization 1, Visualization 2, and Visualization 3 for the changes in one cycle divided into 16 steps in (b), (c), and (d).)

Optics EXPRESS

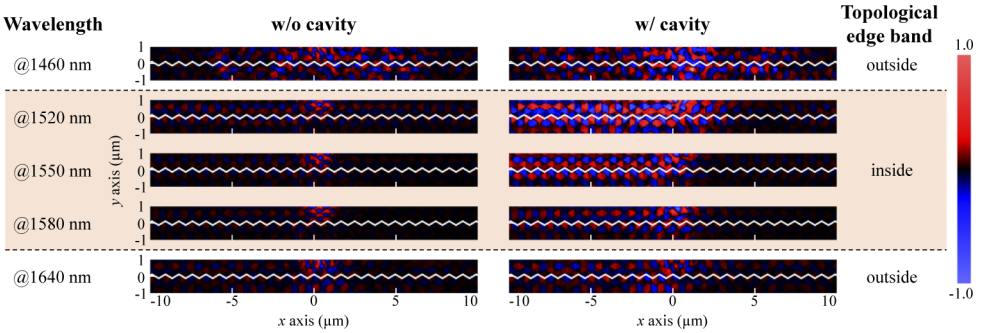


**Fig. 3.** Calculated mode distribution of propagating light at typical wavelengths shown in Fig. 2(a). The white line is the interface between trivial and topological PhCs.

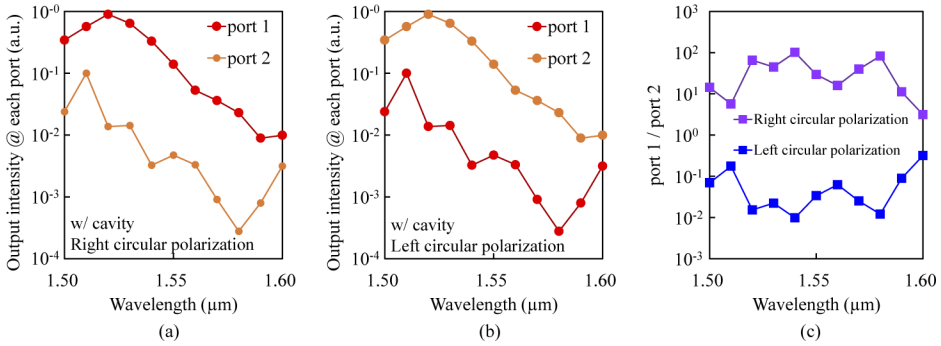


**Fig. 4.** (a) and (b) Wavelength dependence of the output intensity at each port when right and left circularly polarized light is incident on the device, respectively. (c) Ratio between output intensities at the two ports for incident lights with right and left circular polarizations.

shown in Fig. 1. The output at port 1 became dominant when the incident light had right circular polarization, while the output at port 2 became dominant when the incident light had left circular polarization. It was confirmed that the ratio between output intensities of port 1 and port 2 was completely reversed when the direction of circular polarization is switched, the spin-moment-locking characteristics of the topological waveguide.

## 3. Defect position dependence of vertical coupling efficiency

In the previous section, we mentioned that the vertical coupling efficiency of light with circular polarization to the topological waveguide can be improved by introducing a defect structure at the position A shown in Fig. 5(a) (See also Fig. 1(b)). In this section, we analyze how the coupling efficiency depends on where the defect structure is placed in the device, with the results displayed in Fig. 5(b). While, as mentioned in Sec. 2, the defect at position A induces a large improvement in coupling efficiencies over the band (1500–1550 nm) where the topological edge state occurs, the improvements induced by the defect at position B and C are much smaller. For position D, the coupling efficiency was extremely low no matter whether the defect was introduced on not.

These results can be understood from the wavefunction distribution of the topological interface state in the present device. As shown in Fig. 2(b), the topological interface state transporting a net leftwards energy flow is associated with the up pseudospin [9], where the electromagnetic (EM) energy flows counterclockwise in individual unit cells. In order to compose the net interface energy flow from locally whirling energy flows, the wavefunction amplitude is stronger/weaker

Optics EXPRESS

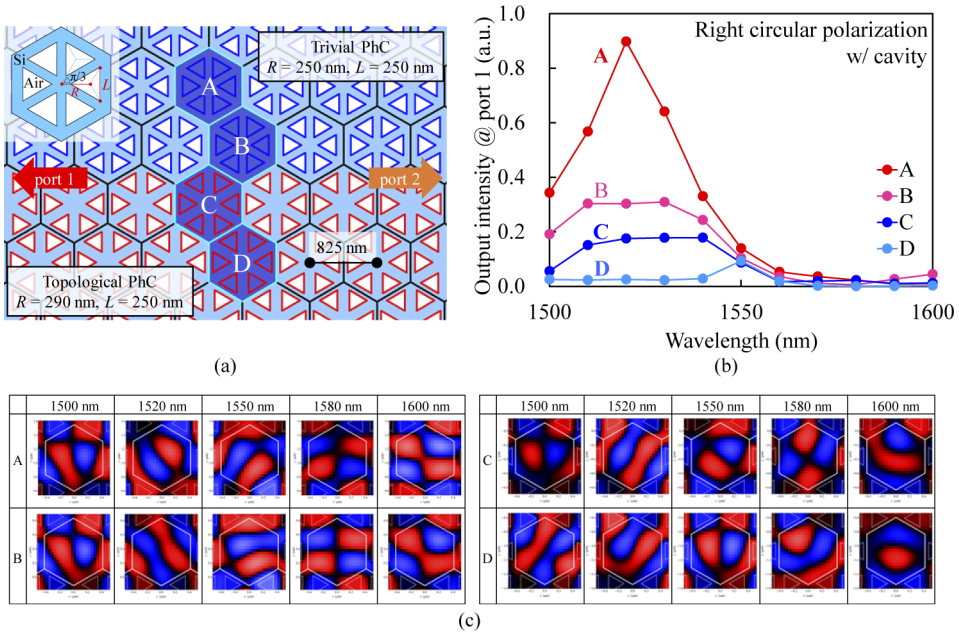


**Fig. 5.** (a) Positions of the defect close to the topological waveguide used in simulations. (b) Coupling efficiency with the defect, when light is incident in the vertical direction at position A to D shown in (a). (c) Mode distributions ($H_z$) around the defect at typical wavelengths when the defect was at position A to D. (See Visualization 4 for the changes in one cycle divided into 16 steps in (c).)

on the side of unit cell close to the interface in the topological/trivial PhC, as can be read from Fig. 2(b). Because the defect is a dielectric hexagon, it attracts EM fields and thus enhances the wavefunction amplitude around it. This enhancement matches the wavefunction distribution of the topological interface state when the defect is placed at position A. While energy flows in individual unit cells are counterclockwise, the enhanced EM fields create a clockwise energy flow surrounding the defect at position A, which contributes positively to the leftwards topological interface energy flow. Therefore, the defect at position A is not harmful for the topological interface state. Inside the dielectric defect, the wavefunction takes a *p*-mode, since a *d*-mode would take a higher energy caused by additional nodes, whereas a *s*-mode obviously cannot match with the phase winding associated with the energy flow, which can be clearly seen in Fig. 2(b) (See also Fig. 2(c)). As shown in Figs. 2(c) and 2(d), the defect *p*-mode takes a mode distribution almost same to the incident beam of right circular polarization with size same as the unit cell. Therefore, an incident beam with right circular polarization creates a strong leftwards, pseudospin-up topological interface state, as shown in Fig. 3.

The *p*-mode in the defect at position A is well localized for frequencies close to the upper band edge, where bulk states are of the *d*-band feature [9], which enhances the coupling between the defect and the topological interface state. For frequencies close to the lower band edge, the defect wavefunction is more extended, since the defect mode and bulk states share the same *p*-mode feature, which weakens the coupling efficiency between the defect and the topological interface state. This is consistent with the wavelength dependence of coupling efficiency shown in Fig. 5(b), where the maximum is taken at the frequency with a short wavelength in the bulk bandgap.

While position D is dual to position A with respect to the zig-zag interface between the topological and trivial PhCs (See Fig. 5(a)), the topological interface state takes a much weaker

Optics EXPRESS

wavefunction around the dielectric defect D as can be seen clearly in Fig. 2(b)). This reduces significantly the coupling between the incident wave and the topological interface state.

As for positions B and C, the defect attracts uniformly EM waves and thus disturbs substantially the topological interface state for which non-uniformity in wavefunction amplitude is crucial for the unidirectional transport EM energy as discussed above. This hampers a strong the coupling between the vertical incident beam and the topological interface state.

Figure 5(c) shows the mode distributions ($H_z$) around the defect for typical wavelengths when the defect was at position A to D. In the wavelength range where coupling efficiency was high, the mode distribution inside the defect was almost the same as that of the incident beam, which allows efficient conversion from the incident circularly polarized beam to the guided wave passing through the topological waveguide as mentioned in Sec. 2. In a sharp contrast, the mode distribution was significantly different from that of the incident beam in the wavelength range where the coupling efficiency was quite low.

## 4. Operating wavelength control

The above-mentioned device achieves a large vertical coupling efficiency at a wavelength of 1520 nm. It is ideal if one can obtain an enhanced coupling efficiency at the desired wavelength. In this section, we show that the wavelength achieving the maximum vertical coupling efficiency (i.e., operating wavelength) can be tuned by adjusting the dielectric arrangement around the defect structure.

A detailed model is described in Fig. 6(a). Here, we considered push away the centers six hexagonal unit cells adjacent to the defect structure to $a(>a_0)$. Figure 6(b) shows the calculated output intensity at port 1 when a right circularly polarized light is incident on a device with the above modification to the device shown in Fig. 1(b). The operating wavelength and $Q$ factor ($Q = \omega_0/\mathrm{FWHM}$, with $\omega_0$ for the frequency with maximum output intensity and FWHM for the full width at half maximum) as functions of $a$ are displayed in Fig. 6(c). Up to $a = 880$ nm, no significant change was observed in the operating wavelength, whereas the $Q$ factor was improved (a tendency similar to that of photonic crystal microcavities [52]). For $a$>880 nm, it was found that the operating wavelength shifted towards longer wavelengths. This is because lateral resonance occurs in the defect, and the resonance wavelength changes as the distance from the nearest dielectric increases. In this way, we demonstrate that the operating wavelength can be controlled over the entire C band.

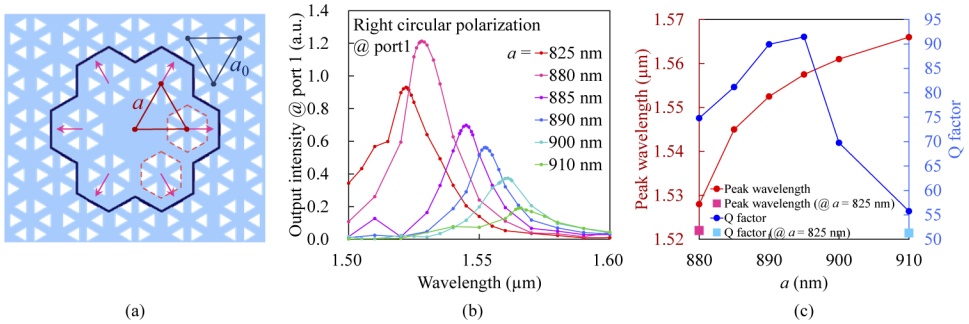


**Fig. 6.** (a) Modified defect structure for controlling the operating wavelength. (b) Calculated output intensity at port 1 when a right circularly polarized light is incident on the device. (c) Operating wavelength and $Q$ factor as a function of the parameter $a$.

Optics EXPRESS

## 5. Conclusions

In this paper, we have proposed introducing a defect structure at the judiciously chosen position to realize highly efficient coupling of light beam with circular polarization vertically incident from free space to topological waveguides. Specifically, we constructed a topological waveguide by interfacing a topological photonic crystal and a trivial one, both formed by triangle nanoholes arranged in honeycomb-type structures respecting $C_{6v}$ symmetry, and introduced a defect structure at the optimized position close to the topological waveguide where the six nanoholes in a specific hexagonal unit cell were removed.

Based on three-dimensional FDTD analysis a significant improvement in the vertical coupling efficiency was observed for the entire telecom C band (4460%@1530 nm). In addition, it was also found that the wavelength showing maximum coupling efficiency can be controlled for the entire C band by tuning the arrangement of the dielectric around the defect structure. These results are considered to be promising for the future construction of topological photonic integrated circuits (TPICs).

**Funding.** Core Research for Evolutional Science and Technology (JPMJCR15N6, JPMJCR18T4); Japan Society for the Promotion of Science (19H02193, 21J14822); Ministry of Internal Affairs and Communications (182103111).

**Acknowledgments.** The authors thank X.-C. Sun and X.-X. Wang for stimulating discussions.

**Disclosures.** The authors declare no conflicts of interest.

**Data availability.** Data underlying the results presented in this paper are not publicly available at this time but may be obtained from the authors upon reasonable request.

## References

1. M. Z. Hasan and C. L. Kane, "Colloquium: topological insulators," Rev. Mod. Phys. **82**(4), 3045–3067 (2010).
2. X.-L. Qi and S.-C. Zhang, "Topological insulators and superconductors," Rev. Mod. Phys. **83**(4), 1057–1110 (2011).
3. D. Xiao, M.-C. Chang, and Q. Niu, "Berry phase effects on electronic properties," Rev. Mod. Phys. **82**(3), 1959–2007 (2010).
4. H. Weng, R. Yu, X. Hu, X. Dai, and Z. Fang, "Quantum anomalous Hall effect and related topological electronic states," Adv. Phys. **64**(3), 227–282 (2015).
5. F. D. M. Haldane and S. Raghu, "Possible Realization of Directional Optical Waveguides in Photonic Crystals with Broken Time-Reversal Symmetry," Phys. Rev. Lett. **100**(1), 013904 (2008).
6. Z. Wang, Y. Chong, J. D. Joannopoulos, and M. Soljacic, "Observation of unidirectional backscattering- immune topological electromagnetic states," Nature **461**(7265), 772–775 (2009).
7. M. Hafezi, S. Mittal, J. Fan, A. Migdall, and J. M. Taylor, "Imaging topological edge states in silicon photonics," Nat. Photonics **7**(12), 1001–1005 (2013).
8. L. Lu, J. D. Joannopoulos, and M. Soljačić, "Topological photonics," Nat. Photonics **8**(11), 821–829 (2014).
9. L.-H. Wu and X. Hu, "Scheme for Achieving a Topological Photonic Crystal by Using Dielectric Material," Phys. Rev. Lett. **114**(22), 223901 (2015).
10. A. B. Khanikaev and G. Shvets, "Two-dimensional topological photonics," Nat. Photonics **11**(12), 763–773 (2017).
11. Y. Wu, C. Li, X. Hu, Y. Ao, Y. Zhao, and Q. Gong, "Applications of Topological Photonics in Integrated Photonic Devices," Adv. Opt. Mater. **5**(18), 1700357 (2017).
12. S. Barik, A. Karasahin, C. Flower, T. Cai, H. Miyake, W. DeGottardi, M. Hafezi, and E. Waks, "A topological quantum optics interface," Science **359**(6376), 666–668 (2018).
13. B.-Y. Xie, H.-F. Wang, X.-Y. Zhu, M.-H. Lu, Z. D. Wang, and Y.-F. Chen, "Photonics meets topology," Opt. Express **26**(19), 24531–24550 (2018).
14. Y. Yang, Y.-F. Xu, T. Xu, H.-X. Wang, J.-H. Jiang, X. Hu, and Z.-H. Hang, "Visualization of a Unidirectional Electromagnetic Waveguide Using Topological Photonic Crystals Made of Dielectric Materials," Phys. Rev. Lett. **120**(21), 217401 (2018).
15. Y. Li, Y. Sun, W. Zhu, Z. Guo, J. Jiang, T. Kariyado, H. Chen, and X. Hu, "Topological LC-circuits based on microstrips and observation of electromagnetic modes with orbital angular momentum," Nat. Commun. **9**(1), 4598 (2018).
16. M. A. Bandres, S. Wittek, G. Harari, M. Parto, J. Ren, M. Segev, D. N. Christodoulides, and M. Khajavikhan, "Topological insulator laser: Experiments," Science **359**(6381), eaar4005 (2018).
17. Z.-K. Shao, H.-Z. Chen, S. Wang, X.-R. Mao, Z.-Q. Yang, S.-L. Wang, X.-X. Wang, X. Hu, and R.-M. Ma, "A high-performance topological bulk laser based on band-inversion-induced reflection," Nat. Nanotechnol. **15**(1), 67–72 (2020).
18. T. Ozawa, H. M. Price, A. Amo, N. Goldman, M. Hafezi, L. Lu, M. C. Rechtsman, D. Schuster, J. Simon, O. Zilberberg, and I. Carusotto, "Topological photonics," Rev. Mod. Phys. **91**(1), 015006 (2019).

Optics EXPRESS


19. M. S. Rider, S. J. Palmer, S. R. Pocock, X. Xiao, P. A. Huidobro, and V. Giannini, "A perspective on topological nanophotonics: Current status and future challenges," J. Appl. Phys. **125**(12), 120901 (2019).
20. E. Verhagen, S. Arora, R. Barczyk, T. A. Bauer, N. Parappurath, and L. K. Kuipers, "Topological protection in photonic crystals," Proc. SPIE **11461**, 1146113 (2020).
21. X.-X. Wang and X. Hu, "Reconfigurable topological waveguide based on honeycomb lattice of dielectric cuboids," Nanophotonics **9**(10), 3451–3458 (2020).
22. S. Iwamoto, Y. Ota, and Y. Arakawa, "Recent progress in topological waveguides and nanocavities in a semiconductor photonic crystal platform," Opt. Mater. Express **11**(2), 319–337 (2021).
23. S. Barik, H. Miyake, W. DeGottardi, E. Waks, and M. Hafezi, "Two-dimensionally confined topological edge states in photonic crystals," New J. Phys. **18**(11), 113013 (2016).
24. E. Yablonovitch, "Inhibited Spontaneous Emission in Solid-State Physics and Electronics," Phys. Rev. Lett. **58**(20), 2059–2062 (1987).
25. J. Joannopoulos, P. Villeneuve, and S. Fan, "Photonic crystals: putting a new twist on light," Nature **386**(6621), 143–149 (1997).
26. T. Baba, "Slow light in photonic crystals," Nat. photonics **2**(8), 465–473 (2008).
27. K. Kondo, T. Tatebe, S. Hachuda, H. Abe, F. Koyama, and T. Baba, "Fan-beam steering device using a photonic crystal slow-light waveguide with surface diffraction grating," Opt. Lett. **42**(23), 4990–4993 (2017).
28. T. Asano, Y. Ochi, Y. Takahashi, K. Kishimoto, and S. Noda, "Photonic crystal nanocavity with a Q factor exceeding eleven million," Opt. Express **25**(3), 1769–1777 (2017).
29. J. B. Pendry, A. J. Holden, D. J. Robbins, and W. J. Stewart, "Magnetism from Conductors and Enhanced Nonlinear Phenomena," IEEE Trans. Microwave Theory Techn **47**(11), 2075–2084 (1999).
30. R. A. Shelby, D. R. Smith, and S. Schultz, "Experimental verification of a negative index of refraction," Science **292**(5514), 77–79 (2001).
31. T. Amemiya, T. Shindo, D. Takahashi, S. Myoga, N. Nishiyama, and S. Arai, "Nonunity Permeability in Metamaterial-based GaInAsP/InP Multimode Interferometers," Opt. Lett. **36**(12), 2327–2329 (2011).
32. N. I. Zheludev and Y. S. Kivshar, "From metamaterials to metadevices," Nat. Mater. **11**(11), 917–924 (2012).
33. T. Amemiya, T. Kanazawa, S. Yamasaki, and S. Arai, "Metamaterial Waveguide Devices for Integrated Optics," Materials **10**(9), 1037 (2017).
34. T. Amemiya, S. Yamasaki, M. Tanaka, H. Kagami, K. Masuda, N. Nishiyama, and S. Arai, "Demonstration of slow-light effect in silicon-wire waveguides combined with metamaterials," Opt. Express **27**(10), 15007–15017 (2019).
35. H. Kagami, T. Amemiya, M. Tanaka, Y. Wang, N. Nishiyama, and S. Arai, "Metamaterial infrared refractometer for determining broadband complex refractive index," Opt. Express **27**(20), 28879–28890 (2019).
36. M. Tanaka, T. Amemiya, H. Kagami, N. Nishiyama, and S. Arai, "Control of slow-light effect in a metamaterial-loaded Si waveguide," Opt. Express **28**(16), 23198–23208 (2020).
37. L. Xu, H.-X. Wang, Y.-D. Xu, H.-Y. Chen, and J.-H. Jiang, "Accidental degeneracy in photonic bands and topological phase transitions in two-dimensional core-shell dielectric photonic crystals," Opt. Express **24**(16), 18059–18071 (2016).
38. Y. Ota, F. Liu, R. Katsumi, K. Watanabe, K. Wakabayashi, Y. Arakawa, and S. Iwamoto, "Photonic crystal nanocavity based on a topological corner state," Optica **6**(6), 786–789 (2019).
39. M. Kim, Z. Jacob, and J. Rho, "Special Issue on "Topological photonics and beyond: novel concepts and recent advances"," Light Sci Appl **9**(1), 203 (2020).
40. M. Kim, Y. Kim, and J. Rho, "Spin-valley locked topological edge states in a staggered chiral photonic crystal," New J. Phys. **22**(11), 113022 (2020).
41. N. Parapppurath, F. Alpeggiani, L. Kuipers, and E. Verhagen, "Direct observation of topological edge states in silicon photonic crystals: Spin, dispersion, and chiral routing," Sci. Adv. **6**(10), eaaw4137 (2020).
42. S. Peng, N. J. Schilder, X. Ni, J. van de Groep, M. L. Brongersma, A. Alù, A. B. Khanikaev, H. A. Atwater, and A. Polman, "Probing the Band Structure of Topological Silicon Photonic Lattices in the Visible Spectrum," Phys. Rev. Lett. **122**(11), 117401 (2019).
43. D. Smirnova, S. Kruk, D. Leykam, E. Melik-Gaykazyan, D.-Y. Choi, and Y. Kivshar, "Third-Harmonic Generation in Photonic Topological Metasurfaces," Phys. Rev. Lett. **123**(10), 103901 (2019).
44. L. Allen, M. W. Beijersbergen, R. J. C. Spreeuw, and J. P. Woerdmanet, "Orbital angular momentum of light and the transformation of Laguerre-Gaussian laser modes," Phys. Rev. A **45**(11), 8185–8189 (1992).
45. R. C. Devlin, A. Ambrosio, D. Wintz, S. L. Oscurato, A. Y. Zhu, M. Khorasaninejad, J. Oh, P. Maddalena, and F. Capasso, "Spin-to-orbital angular momentum conversion in dielectric metasurfaces," Opt. Express **25**(1), 377–397 (2017).
46. N. Bozinovic, Y. Yue, Y. Ren, M. Tur, P. Kristensen, H. Huang, A. E. Willner, and S. Ramachandran, "Terabit-Scale Orbital Angular Momentum Mode Division Multiplexing in Fibers," Science **340**(6140), 1545–1548 (2013).
47. X.-T. He, E.-T. Liang, J.-J. Yuan, H.-Y. Qiu, X.-D. Chen, F.-L. Zhao, and J.-W. Dong, "A silicon-on-insulator slab for topological valley transport," Nat. Commun. **10**(1), 872 (2019).
48. Y. Shen, X. Wang, Z. Xie, C. Min, X. Fu, Q. Liu, M. Gong, and X. Yuan, "Optical vortices 30 years on: OAM manipulation from topological charge to multiple singularities," Light Sci Appl **8**(1), 90 (2019).

Optics EXPRESS


49. Y. Wang, P. Zhao, X. Feng, Y. Xu, K. Cui, F. Liu, W. Zhang, and Y. Huang, "Integrated photonic emitter with a wide switching range of orbital angular momentum modes," Sci. Rep. **6**(1), 22512 (2016).
50. H. Kagami, T. Amemiya, S. Okada, N. Nishiyama, and X. Hu, "Topological converter for high-efficiency coupling between Si wire waveguide and topological waveguide," Opt. Express **28**(22), 33619–33631 (2020).
51. J. Ma, X. Xi, and X. Sun, "Topological Photonic Integrated Circuits Based on Valley Kink States," Laser Photonics Rev. **13**(12), 1900087 (2019).
52. Y. Akahane, T. Asano, B.-S. Song, and S. Noda, "Fine-tuned high-Q photonic-crystal nanocavity," Opt. Express **13**(4), 1202–1214 (2005).